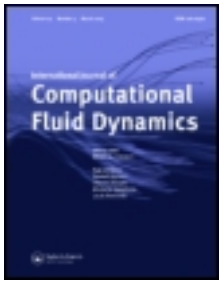

International Journal of Computational Fluid Dynamics
Publication details, including instructions for authors and subscription information:
http://www.tandfonline.com/loi/gcfd20

Reduced order borehole induction modelling

N. Ardjmandpour[a], C.C. Pain[b], F. Fang[b], A.G. Buchan[b], J. Singer[a], M.A. Player[a], Xu Xu[a], I.M. Navon[c] & J. Carter[b]

[a] GE Energy Oilfield Technology, Hampshire, UK

[b] Department of Earth Science and Engineering, Imperial College London, London, UK

[c] Department of Scientific Computing, Florida State University, Tallahassee, FL, USA

Published online: 10 Jun 2014.

To cite this article: N. Ardjmandpour, C.C. Pain, F. Fang, A.G. Buchan, J. Singer, M.A. Player, Xu Xu, I.M. Navon & J. Carter (2014): Reduced order borehole induction modelling, International Journal of Computational Fluid Dynamics, DOI: 10.1080/10618562.2014.923846

To link to this article: http://dx.doi.org/10.1080/10618562.2014.923846

International Journal of Computational Fluid Dynamics, 2014
http://dx.doi.org/10.1080/10618562.2014.923846

Reduced order borehole induction modelling

N. Ardjmandpour[a], C.C. Pain[b], F. Fang[b], A.G. Buchan[b], J. Singer[a], M.A. Player[a], Xu Xu[a], I.M. Navon[c,*] and J. Carter[b]

[a]*GE Energy Oilfield Technology, Hampshire, UK;* [b]*Department of Earth Science and Engineering, Imperial College London, London, UK;* [c]*Department of Scientific Computing, Florida State University, Tallahassee, FL, USA*

(*Received 15 January 2014; accepted 5 May 2014*)

This article presents a new reduced order model based on proper orthogonal decomposition (POD) for solving the electromagnetic equation for borehole modelling applications. The method aims to accurately and efficiently predict the electromagnetic fields generated by an array induction tool – an instrument that transmits and receives electrical signals along different positions within a borehole. The motivation for this approach is in the generation of an efficient 'forward model' (which provides solutions to the electromagnetic equation) for the purpose of improving the efficiency of inversion calculations (which typically require a large number of forward solutions) that are used to determine surrounding material properties. This article develops a reduced order model for this purpose as it can be significantly more efficient to compute than standard models, for example, those based on finite elements. It is shown here how the POD basis functions are generated from the snapshot solutions of a high resolution model, and how the discretised equations can be generated efficiently. The novelty is that this is the first time such a POD model reduction approach has been developed for this application, it is also unique in its use of separate POD basis functions for the real and complex solution fields. A numerical example for predicting the electromagnetic field is used to demonstrate the accuracy of the POD method for use as a forward model. It is shown that the method retains accuracy whilst reducing the costs of the computation by several orders of magnitude in comparison to an established method.

Keywords: POD; reduced order model; array induction tool; Maxwell equations

1. Introduction

Electromagnetic induction tools are used in the oil and gas industry to determine the electrical conductivity (or its converse resistivity) of geological formations which, in turn, indicates the content of hydrocarbons. Boreholes are drilled into regions of interest and downhole measurements made using instruments, such as the array induction tool, that transmit and detect electrical signals along different locations in the hole. The data containing the sent and received signals are processed to provide a profile of the conductivity of the surrounding materials. This can be achieved through the use of computational models and the technique known as inversion.

When using inversion on the measured (induction) signal to estimate the formation conductivity, one uses an iterative optimisation technique based on the solutions of a forward model. A forward model is typically generated from the discretisation of a partial differential equation (PDE) that describes the physics of the problem, and popular discretisation techniques include the finite element method (FEM) and finite difference methods, to mention but a few. However, if the complexity of the problem is such that high modelling resolution is required, solutions from these types of models can become expensive to compute. The result is that the overall inversion process, which often requires many forward model solutions, may take exceptionally long times to solve (Lin, Gianzera, and Strickland 1984).

In an attempt to reduce the computational expense of a forward model, early work includes that of Anderson and Gianzero (1983) who developed a one-dimensional spectral integral technique. This computed induction responses through media with an arbitrary number of planar layers. Although this was successful in improving the speed of the calculation, compared to (say) the FEM (Lin, Gianzera, and Strickland 1984; Dyos 1987; Freedman and Minerbo 1991), these models were still too inefficient for realistic use in well-site identification. Simplification techniques have also been introduced including that of the Born approximation (Thadani, Merchant, and Verbout 1983). This used the method of geometrical factor theory (Doll 1949; Moran 1982) and was successful in providing a considerable speed up of the inversion process (Dyos 1987; Freedman and Minerbo 1991). This method however did have its drawbacks in that it would break down in highly conductive beds, or where the problem contained large variations in conductivity. Other methods for improving the efficiency of inversion include the substitution of the forward model with a neural network. This approach

* Corresponding author. Email: inavon@fsu.edu

used the layered conductivities as its inputs and the array responses as the outputs. Whilst being relatively successful for improving efficiency, a large training set was required in order for it to resolve the range of conductivities seen in bed formations. This was partially resolved in the thesis of Ardjmandpour (2010) enabling the efficient collection of training data, but even this method had its limitations.

In this article a new approach is described for the efficient implementation of a forward model based on a reduced order model using the method of proper orthogonal decomposition (POD). This approach is attractive to this field of research as it has the ability to extract optimal basis functions for a dynamic system based on information of its experimental data or numerical solutions. Specifically it extracts the most energetic modes of the data and forms its basis functions that recover this information in the most efficient way. In this paper the data used to form the model are based on the method of snapshots, Sirovich (1987). This uses the numerical solutions from a high resolution model.

The origins of POD date back to the early work of Pearson (1901) and since then the method has developed under other names such as principal component analysis (Kosambi 1943; Fukunaga 1990) (in statistics), the Karhunen–Loève decomposition (Loève 1945; Karhunen 1946), drill string dynamics (Liao et al. 2011) and empirical orthogonal functions (used in oceanography and meteorology) (Jolliffe 2002; Crommelin and Majda 2004; Majda, Timofeyev, and Vanden-Eijnden 2003). It has been used successfully in several fields including those of fluid dynamics and coherent structures (Lumley 1967; Aubry, Holmes, and Lumley 1988; Holmes, Lumley, and Berkooz 1998; Willcox and Peraire 2002), signal processing and pattern recognition (Fukunaga 1990), image reconstruction (Kirby and Sirovich 1990), inverse problems (Vauhkonen et al. 1997; Banks et al. 2000; Hopcroftand et al. 2009) and ocean modelling. Recent work has also combined this method within the four-dimensional variational (4D-Var) data assimilation technique (Robert et al. 2005; Hoteit and Köhl 2006; Luo et al. 2007; Fang et al. 2009; Cao et al. 2007). POD is particularly effective and simple to use with linear PDEs, and methods have been developed for their use with non-linear equations in order to maintain efficiency. Such methods include quadratic expansion, Gauss-Newton with approximated tensors (GNAT) (Carlberg et al. 2013) and Discrete Empirical Interpolation Method (DEIM) (Chaturantabut and Sorensen 2010), and more recent work includes the hybrid approach residual-DEIM (combining the quadratic expansion and DEIM) (Xiao et al. 2014). Other works that aim to maintain effectiveness of the method include those centred on optimally selecting snapshot sets, as this has profound impacts on the resulting POD models (Gunzburger 2003). This includes the work of the dual-weighed approach (Daescu and Navon 2008; Chen, Navon, and Fang 2011; Kunisch and Volkwein 2010) and also that of Kunisch and Volkwein (2010). This article expands this extensive list of applications by developing the first POD method for solving the electromagnetic equations used in downhole measurements. This involves the reduced order modelling of a linear PDE; however, it is complex in nature and so requires separate POD functions for the real and complex terms of the equation.

As previously mentioned the POD model developed here is constructed through the method of snapshots which comprises a collection of solutions generated by a high resolution model. For this the finite element based COMSOL model[1] is employed. A sequence of solutions are generated by solving the electromagnetic equation (the solutions being the azimuthal magnetic vector potentials) on problems based on domains that mimic those seen in borehole experiments. Essentially this applies a charge within a domain that allows the electromagnetic field to interact with its surrounding materials, and how this interacts depends on the material's electrical properties. The snapshot solutions are created by repeated solves of the equation using different electrical properties of the surrounding materials – in these examples conductivities are layered and vary as a function of depth. Once these solutions are collected the POD basis functions and their associated discretised equations are generated through the standard singular value decomposition (SVD) approach. In this article the technique developed in Fang et al. (2009, 2011) is applied for the efficient generation of the POD model equations.

The sections of this article are structured as follows. Section 2 provides a brief introduction to array induction tools followed by a description of the governing electromagnetic equations. Section 3 details the POD method generated through the method of snapshots and generates the reduced order model for the application of solving the electromagnetic equations. Section 4 presents some numerical examples applying the POD models and conclusions are drawn in Section 5.

2. Induction tools

2.1. *Fundamental aspects*

Commercial induction tools are normally composed of several transmitter and receiver coils. Their basic element is a two-coil sonde consisting of a transmitter and a receiver mounted coaxially on a mandrel, as shown in Figure 1. It functions by applying a constant-amplitude alternating current to the transmitter coil to form a primary electromagnetic field around the tool. This, in turn, induces eddy currents (often called 'ground loops') within the formation (i.e. the material surrounding the tool), which flow coaxially to the borehole and have intensity proportional to the material's conductivity. From these eddy currents a secondary voltage is induced within the receiver coil, and through the use of 'bucking coils' the voltage that would arise directly from the transmitter is eliminated. The induced voltage at the receiver is therefore a result of only the electromagnetic

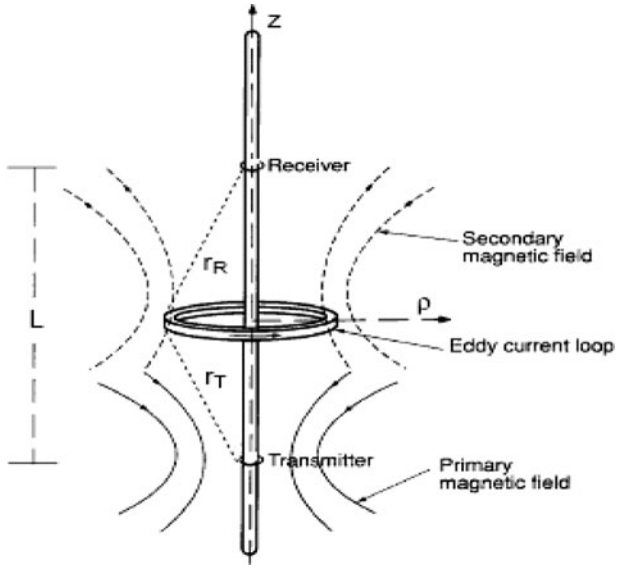

Figure 1. Basic two-coil induction tool. The vertical component of the magnetic field from the transmitter coil induces ground loop currents. The current loops in the conductive formation produce a secondary magnetic field detected by the receiver coil (Anderson 2001).

field from within the media. This information allows us to probe the media and investigate its electrical properties.

The magnetic field induced by the transmitter is affected by several factors associated with the logging environment, some of which are illustrated in Figure 2. These include the effects due to the presence of the borehole, mud filtration (mud from the borehole entering the media), shoulder effects (conductivities in regions above and below the regions of interest) and dipping beds (non-horizontal layers that smear voltage responses, Barber et al. 1999). These effects must be accounted for, and some correction method applied, in order to accurately estimate the formation conductivity. Quite often, in the past, it came down to the experience of the log analyst to make such corrections, others used a series of correction charts (Rust and Anderson 1975; Anderson 2001; Hardman and Shen 1987). However from the mid 1980s the use of computer modelling made it possible for the log analyst to use correction algorithms based on forward modelling, Anderson (2001).

Grove and Minerbo, in 1991, designed a correction algorithm to solve for borehole parameters by minimising the difference between the model and measured signals from array induction tool. The borehole corrected signals were combined to form the log responses which had the desired vertical response, radial response and a smooth near-borehole two-dimensional (2D) response (Barber and Rosthal 1991; Ellis and Singer 2007). With this a 2D inversion method was then used to estimate the formation conductivity and invasion parameters, that is, invasion conductivity and invasion radius (Howard 1992). In horizontal and deviated wells the dip correction algorithm, based on filtering (Xiao, Geldmacher, and Rabinovich 2000), and the iterative inversion (Barber et al. 1999) have been developed to remove the 'dip effects'.

2.2. *The governing electromagnetic equation*

This article considers the 2D electromagnetic equation, which is expressed as

$$\left(i\omega\sigma - \omega^2\varepsilon_0\varepsilon_r\right) A_\phi(r,z) + \nabla \times \left(\mu_0^{-1}\mu_r^{-1}\nabla \times A_\phi(r,z)\right) = J_\phi^e(r,z) \quad (1)$$

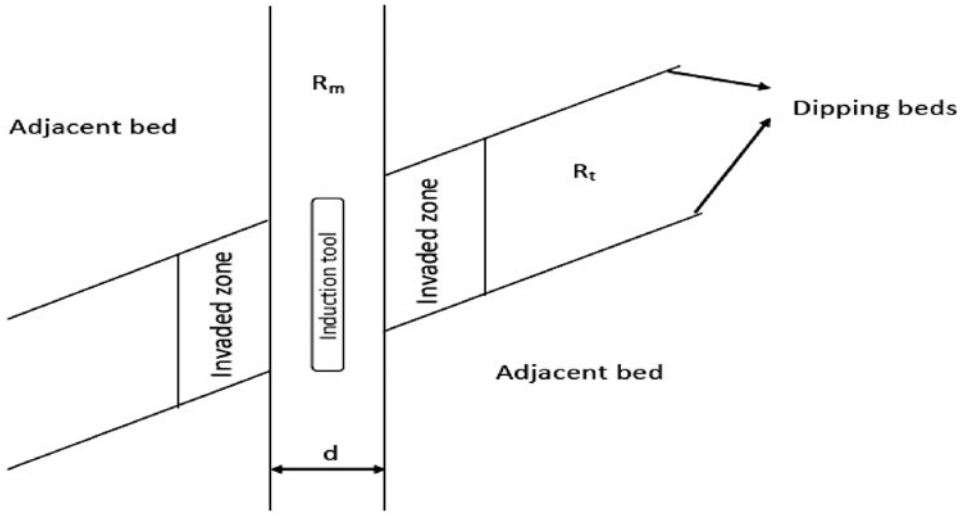

Figure 2. The logging environment such as mud conductivity and borehole size, mud filtrate invasion, adjacent bed and dipping beds affect the measured signal. To estimate the true formation conductivity, one needs to correct for these effects.

in terms of the solution variable $A_\phi(r, z)$. This variable defines the azimuthal vector potential as a function that varies with radial distance (r) (from the borehole) and vertical depth (z). The potential arises as a result from an external current density (i.e. the source term initiated from the induction tool) which is denoted as $J^e_\phi(r, z)$. Of the several parameters within the equation the terms ω denote the current frequency and μ_r the formation's relative magnetic permeability. The term σ denotes the formation conductivity and ε_r is the relative dielectric permittivity. μ_0 and ε_0 are the magnetic permeability and the dielectric permittivity of free space, respectively. As this paper is only concerned with a forward model, it is the solution A_ϕ that is being sought here. Therefore remaining variables, which are the properties of the materials contained within the problem domain, are considered to be known.

Given the solution A_ϕ across the domain of interest, the voltage induced within a receiver coil is calculated from the relation, $E = i\omega A_\phi$, where E is the electric field strength. For a receiver coil that has radius ρ and N_R turns, the induced voltage is given as

$$V = 2\pi\rho N_R E = 2\pi\rho N_R i\omega A_\phi. \tag{2}$$

The model COMSOL is employed to generate the full solutions of Equation (1), and from this the snapshots for generating the POD model are recorded. COMSOL uses linear finite element functions on triangular element meshes to discretise the 2D domain. Its approximation of A_ϕ is written as

$$A_\phi(r, z) = \sum_{i=1}^{N} \mathcal{N}_i(r, z) A_{\phi_i}, \tag{3}$$

where $\mathcal{N}$ denotes the finite element functions, $A_{\phi i}$ are the corresponding coefficients and N denotes the size of the expansion. The discretisation generates a linear system through a weighted residual approach. Equation (1) is weighted with each finite element function, the solution replaced with its approximation and whole system integrated over space,

$$\begin{aligned}\int_\Omega N_j(r, z)\Bigg((i\omega\sigma - \omega^2\varepsilon_0\varepsilon_r)\left(\sum_{i=1}^{N}\mathcal{N}_i(r, z)A_{\phi_i}\right)\\ + \nabla\times\left(\mu_0^{-1}\mu_r^{-1}\nabla\times\left(\sum_{i=1}^{N}\mathcal{N}_i(r, z)A_{\phi_i}\right)\right.\\ \left. - J^e_\phi(r, z)\Bigg)d\Omega = 0,\ j \in \{1, 2, \ldots, N\}.\end{aligned} \tag{4}$$

This system can be expressed as the following linear system:

$$E(\sigma)A_\phi = b, \tag{5}$$

where $E(\sigma)$ is an $N \times N$ matrix (containing the discretised terms on the left side of Equation (1)), b is a vector of size N containing the discretised source and A_ϕ is a vector of size N containing the coefficients of Equation (3). In an attempt to reduce notation between working in continuous and discrete spaces, when the solution variables are expressed with (r, z) then they are being referred to as continuous variables (as Equation (4)), else they will be assumed to be discrete (as in Equation (5)).

3. Construction of the POD model from a snapshot data set

The full model described in the previous section is used to provide solutions (called snapshots) of the electromagnetic equation for problem domains with varying material properties. These solutions are collected together to provide what is called a snapshot data set. As the solutions can be regarded as the coefficients of the finite element expansion, each of these snapshots is simply a vector A_ϕ, as defined in Equation (5). The snapshot matrix $\mathcal{A}$ is defined to represent all the solution data by storing each snapshot, each in turn, in its columns. That is, the ith snapshot taken of A_ϕ forms the ith column of $\mathcal{A}$. This matrix therefore has dimensions $N \times K$, where N is the size of the finite element expansion and K the number of snapshots (or solutions) recorded.

In the POD approach the average of the collection of snapshots is defined as

$$\bar{\mathcal{A}} = \frac{1}{K}\sum_{k=1}^{K}\mathcal{A}_k, \tag{6}$$

where $\bar{\mathcal{A}}$ is a vector of size N and $\mathcal{A}_k$ is the kth column vector of the snapshot matrix $\mathcal{A}$. A modified matrix $\tilde{\mathcal{A}}$ is now defined, where each of its column vectors, $\tilde{\mathcal{A}}_k$, is expressed as

$$\tilde{\mathcal{A}}_k = \mathcal{A}_k - \bar{\mathcal{A}}. \tag{7}$$

Essentially this is just the original snapshot matrix with the mean column vector removed.

POD now sets out to find a set of orthogonal basis functions that best spans this data set. A simple way of achieving this is through the SVD of the matrix $\tilde{\mathcal{A}}$. Without going into excessive detail, $\tilde{\mathcal{A}}$ is represented by its SVD,

$$\tilde{\mathcal{A}} = U\Sigma V^t, \tag{8}$$

where U and V are unitary matrices (with dimensions $N \times N$ and $K \times K$, respectively) and Σ a diagonal matrix (dimensions $N \times K$) containing the singular values (arranged in descending order of magnitude). It is shown, from the well-developed theory, that choosing the first set of M singular values, and zeroing out the rest, provides the optimal

reduced representation of this matrix (in the sense that no other rank M matrix can produce a closer representation). From this fact, it can also be shown that the first M column vectors of U define the optimal basis vectors, and it is these vectors that define the POD basis functions. That is, the vectors $\Phi_i = U_i, i \in \{1, 2, \ldots M\}$, where U_i denotes the ith column of U, are defined as the POD vectors which are of size N. These POD vectors can be used to reconstruct the corresponding POD functions through the finite element representation,

$$\Phi_j(r, z) = \sum_{i=1}^{N} \mathcal{N}_i(r, z)[\Phi_j]_i, \tag{9}$$

and a similar expression can be written for the average snapshot vector, that is,

$$\bar{\mathcal{A}}(r, z) = \sum_{i=1}^{N} \mathcal{N}_i(r, z)\bar{\mathcal{A}}_i. \tag{10}$$

Together Equations (9) and (10) can be combined to form an expansion of the continuous solution variables in terms of POD functions,

$$A_{\Phi}^{\mathrm{POD}}(r, z) = \bar{\mathcal{A}}_{\Phi}(r, z) + \sum_{m=1}^{M} \Phi_m(r, z)\mathrm{a}_m, \tag{11}$$

where a_m are the expansion coefficients. Alternatively, in terms of a discrete representation this expansion can be written as

$$A_{\Phi}^{\mathrm{POD}} = \bar{\mathcal{A}} + \sum_{i=1}^{M} \Phi_m \mathrm{a}_m, \tag{12}$$

which expresses the solution in terms of the finite element expansion coefficients.

A measure of the expected quality of the approximation can be gained from the calculation of its *energy*. This is defined as the ratio of sum of singular values that were retained vs. the sum of total number of eigenvalues,

$$I(M) = \frac{\sum_{i=1}^{M} \Lambda_{i,i}}{\sum_{i=1}^{\ell} \Lambda_{i,i}}, \tag{13}$$

where $\Lambda_{i,i} = \Sigma_{i,i}^2$. This value varies between 0 and 1 (1 being a complete recovery) and provides a guide to how much information of the snapshot data the POD functions will capture.

3.1. The POD discretisation of the electromagnetic equations

The POD model of the electromagnetic equation can now be derived through a Galerkin projection on Equation (1). The equation is weighted with each POD function, the vector potential is replaced with its POD representation (11) and the whole system is integrated over space. This results in the following system:

$$\int_{\Omega} \Phi_j(r, z) \Bigg((i\omega\sigma - \omega^2 \varepsilon_0 \varepsilon_r) \left(\bar{\mathcal{A}}(r, z) + \sum_{m=1}^{M} a_m \, \Phi_m(r, z) \right) + \nabla \times \left(\mu_0^{-1} \mu_r^{-1} \nabla \times \left(\bar{\mathcal{A}}(r, z) + \sum_{m=1}^{M} a_m \, \Phi_m(r, z) \right) \right) - J_{\phi}^{e}(r, z) \Bigg) d\Omega = 0, \tag{14}$$

for each POD function $j \in \{1, 2, \ldots, M\}$. Analogous to the full model derivation, this can also be recast into a linear system of equations,

$$\hat{E}(\sigma)\mathbf{a} = \hat{b}, \tag{15}$$

where $\hat{E}(\sigma)$ is an $M \times M$ matrix containing the discretised terms of Equation (14), $\hat{b}$ is the vector of size M containing the discretised source and $\mathbf{a}$ the vector of size M containing the POD coefficients. This linear system can also be calculated directly from the discrete form if the original finite element linear system of equations (5) is available,

$$\begin{aligned} \hat{E}(\sigma) &= \Phi^T E(\sigma) \Phi, \\ \hat{b} &= \Phi^T b. \end{aligned} \tag{16}$$

That is, the entries of the matrix $\hat{E}(\sigma)$ (and the elements of the vector $\hat{b}$) can be constructed from the entries of the matrix E (and vector b) by the relationships

$$\hat{E}_{m,l}(\sigma) = \sum_{p=1}^{N} \sum_{q=1}^{N} E_{p,q}(\sigma) \Phi_{m,p} \Phi_{l,q}, \tag{17}$$

$$\hat{b}_m = \sum_{p=1}^{N} b_p \Phi_{m,p}. \tag{18}$$

A problem now arises with regards to the efficient construction of the linear system through relationships (17) and (18). This is because each POD model requires a new full system of equations to be formed, and its reduction through the matrix–matrix multiplications is expensive to compute. In fact the computational costs are such that the procedure will remove the benefits from solving on the reduced POD space. To overcome this, this article uses

the approach developed by Fang et al. (2009, 2011) which constructs the full system of equations from the sum of a set of reference system of equations

$$E(\sigma) = E_0 + \sum_{l=1}^{L} \sigma^l (E_1^l - E_0). \tag{19}$$

In this expression the matrix E_0 is derived from Equation (1) using the material property $\sigma = 0$. The summation in the expression relates to the number of layers present in the problem, here this is assumed to be L, and a matrix E_1^l is defined for each of these layers. E_1^l in fact only has non-zero components that contribute to its level. That is, in the finite element discretisation, if an element is within the region of layer l then its contribution gets added to E_1^l, else it is ignored. When contributing to each matrix E_1^l the value of the conductivity is set to $\sigma = 1$. One can now see that in the summation, involving the multiplication of $(E_1^l - E_0)$ by the conductivity of the layer σ_l, the exact full system is reproduced. The operations defined in Equations (17) and (18) can now be performed on these reference matrices, and since these can be pre-computed and their numbers are generally small, this process is efficient. From these reduced reference matrices the POD model can be generated from their summation in a form analogous to that in Equation (19).

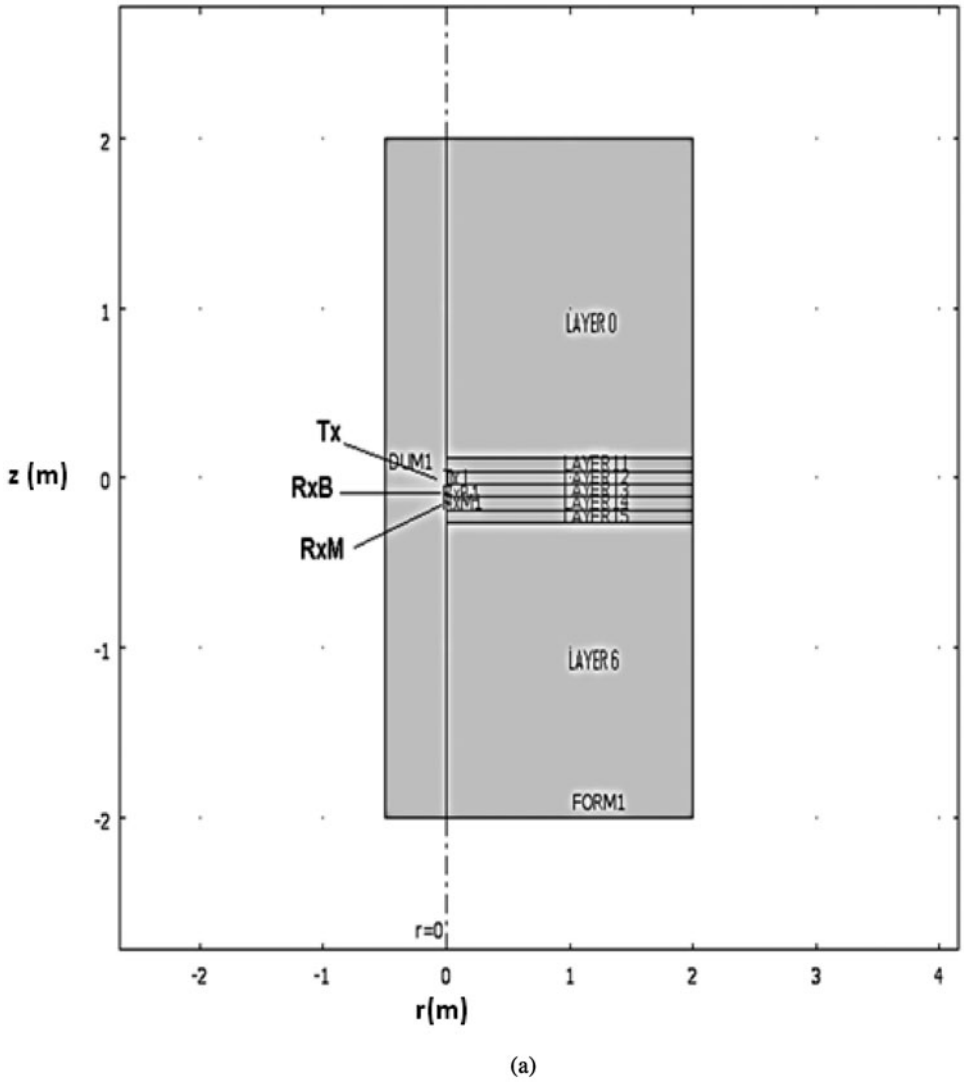

(a)

Figure 3. Layered media to be modelled to generate the required snapshots for POD model reduction. We assume that the data are borehole corrected, therefore the borehole is not included in the model. Layer thickness (layers 1–5) is 0.07 m (3 inch). The transmitter coil (Tx) is situated within layer 2 and main (RxM) and bucking (RxB) coils are located 0.15 m (6 inch) and 0.1 m (4 inch), respectively, from Tx. The solution is calculated as the azimuthal component of magnetic vector potential A_ϕ, the model imposes the Dirichlet boundary conditions $A_\phi = 0$ on the symmetry axis.

3.2. Forming the complex POD reduced order model

The linear system defined by Equation (5) is complex and has a complex solution; it may therefore be written as

$$(P + i\ Q)(A_{\Phi,R} + i\ A_{\Phi,I}) = (b_R + i\ b_I)$$

or in a matrix form as

$$\begin{pmatrix} P & -Q \\ Q & P \end{pmatrix} \begin{pmatrix} A_{\Phi,R} \\ A_{\Phi,I} \end{pmatrix} = \begin{pmatrix} b_R \\ b_I \end{pmatrix}. \tag{20}$$

Here the matrices P and Q are the real and imaginary parts of full matrix E, respectively. The subscript R and L relate the solution and source vectors to their real part and imaginary parts, respectively.

In order to generate representative POD functions for the system of equations (20), separate POD functions are created for the real and imaginary terms of its solution. The creation of the POD discretisation therefore applies the SVD procedure to two sets of snapshot matrices, namely $\mathcal{A}_{\mathcal{R}}$ and $\mathcal{A}_I$, that contain the real and imaginary parts of the full snapshot solutions. By following the previous section, two vectors are generated, namely $\bar{\mathcal{A}}_R$ and $\bar{\mathcal{A}}_I$, that represent the average of these two snapshot sets. From these the modified matrices $\tilde{\mathcal{A}}_R$ and $\tilde{\mathcal{A}}_I$ (denoting the real and imaginary) are created by removing from the columns of the original snapshots these average vectors. The POD vectors are generated by applying the SVD upon these modified matrices, these are denoted as $(\Phi_R)_i$ and $(\Phi_I)_i$, for $i \in \{1, 2, \ldots M\}$, respectively, which when concatenated together, column by column, form the matrices Φ_R and Φ_I.

A new set of POD basis vectors Φ is formed from the real and imaginary POD basis vectors,

$$\Phi = \begin{pmatrix} \Phi_R & 0 \\ 0 & \Phi_I \end{pmatrix} \tag{21}$$

and these are used to pre- and post-multiply (as with Equation (16)) with the full linear system in Equation (20). The reduced linear system can be written as

$$\hat{E}(\sigma) = \Phi^T E(\sigma)\Phi = \begin{pmatrix} \Phi_R^T P \Phi_R & -\Phi_R^T Q \Phi_I \\ \Phi_I^T Q \Phi_R & \Phi_I^T P \Phi_I \end{pmatrix}, \tag{22}$$

and, in the form of the summation defined in Equation (19), this reads as

$$\begin{pmatrix} \Phi_R^T P_0 \Phi_R + \sum_{l=1}^{L} \sigma^l (\Phi_R^T P_1^l \Phi_R - \Phi_R^T P_0 \Phi_R) & -(\Phi_R^T Q_0 \Phi_I + \sum_{l=1}^{L} \sigma^l (\Phi_R^T Q_1^l \Phi_I - \Phi_R^T Q_0 \Phi_I)) \\ \Phi_I^T Q_0 \Phi_R + \sum_{l=1}^{L} \sigma^l (\Phi_I^T Q_1^l \Phi_R - \Phi_I^T Q_0 \Phi_R) & \Phi_I^T P_0 \Phi_I + \sum_{l=1}^{L} \sigma (\Phi_I^T P_1^l \Phi_I - \Phi_I^T P_0 \Phi_I) \end{pmatrix}, \tag{23}$$

where P_0 and Q_0 are the real and imaginary parts (respectively) of E_0 with $\sigma = 0$. Similarly the matrices P_1^l and Q_1^l are the real and imaginary parts (respectively) of E_1 relating to level l and with material $\sigma = 1$.

Table 1. The 27 best runs of three values of conductivities (0.001, 0.03 and 1 S/m) for five layers determined based on the fractional factorial design (Xu 2005).

No of cases	Layer 1	Layer 2	Layer 3	Layer 4	Layer 5
1	0.001	0.001	0.001	0.001	0.001
2	0.001	0.001	0.03	0.03	0.001
3	0.001	0.001	1	1	0.001
4	0.001	0.03	0.001	0.03	1
5	0.001	0.03	0.03	1	1
6	0.001	0.03	1	0.001	1
7	0.001	1	0.001	1	0.03
8	0.001	1	0.03	0.001	0.03
9	0.001	1	1	0.03	0.03
10	0.03	0.001	0.001	0.03	0.03
11	0.03	0.001	0.03	1	0.03
12	0.03	0.001	1	0.001	0.03
13	0.03	0.03	0.001	1	0.001
14	0.03	0.03	0.03	0.001	0.001
15	0.03	0.03	1	0.03	0.001
16	0.03	1	1	0.001	1
17	0.03	1	0.03	0.03	1
18	0.03	1	1	1	1
19	1	0.001	0.001	1	1
20	1	0.001	0.03	0.001	1
21	1	0.001	1	0.03	1
22	1	0.03	0.001	1	0.03
23	1	0.03	1	0.03	0.03
24	1	0.03	1	1	0.03
25	1	1	0.001	0.03	0.001
26	1	1	1	1	0.001
27	1	1	0.001	0.001	0.001

The Right Hand Side (RHS) vector $\hat{b}$ is composed of both the discretised source and the term involving the mean vector $\bar{A}$. When pre-multiplied by the Φ^T its expression reads as

$$\hat{b} = \Phi^T (b - E(\sigma)\bar{A}), \tag{24}$$

which, when expanded out in terms of the real and imaginary components, is given as

$$\begin{pmatrix} \Phi_R^T b - \Phi_R^T P \bar{A}_R + \Phi_R^T Q \bar{A}_I \\ -\Phi_I^T Q \bar{A}_R - \Phi_I^T P \bar{A}_I \end{pmatrix}. \tag{25}$$

Again using the summing technique described in Equation (19), the expression for the source terms in the POD system

reads as

$$\begin{pmatrix} \Phi_R^T b - \left(\Phi_R^T P_0 \bar{A}_R + \sum_{l=1}^{L} \sigma^l (\Phi_R^T P_1^l \bar{A}_R - \Phi_R^T P_0 \bar{A}_R)\right) + \left(\Phi_R^T Q_0 \bar{A}_I + \sum_{l=1}^{L} \sigma^l (\Phi_R^T Q_1^l \bar{A}_I - \Phi_R^T Q_0 \bar{A}_I)\right) \\ -\left(\Phi_I^T P_0 \bar{A}_I + \sum_{l=1}^{L} \sigma^l (\Phi_I^T P_1^l \bar{A}_I - \Phi_I^T P_0 \bar{A}_I)\right) - \left(\Phi_I^T Q_0 \bar{A}_R + \sum_{l=1}^{L} \sigma^l (\Phi_I^T Q_1^l \bar{A}_R - \Phi_I^T Q_0 \bar{A}_R)\right) \end{pmatrix}. \quad (26)$$

Together the expressions given in Equations (23) and (26) can be condensed into the form

$$\begin{pmatrix} \hat{P} & -\hat{Q} \\ \hat{Q} & \hat{P} \end{pmatrix} \begin{pmatrix} \mathbf{a_R} \\ \mathbf{a}_I \end{pmatrix} = \begin{pmatrix} \hat{b}_R \\ \hat{b}_I \end{pmatrix}. \quad (27)$$

Here the vectors $\mathbf{a}_I$ and $\mathbf{a}_R$ are the coefficients for the reduced order model expressing the solution in its real and complex parts. The system is of dimension $2M \times 2M$ where $M \ll N$ and, more importantly, the elements of the systems and RHS can be constructed efficiently.

The coefficients of the original Finite Element (FE) expansion can be recovered using the relationship

$$\begin{aligned} A_R^{\text{POD}} &= \bar{A}_R + \Phi_R^T \mathbf{a}_R; \quad \text{real part,} \\ A_I^{\text{POD}} &= \bar{A}_I + \Phi_I^T \mathbf{a}_I; \quad \text{imaginary part.} \end{aligned} \quad (28)$$

4. Numerical experiments

In this section a demonstration of the capabilities of the POD model is provided by its application to solving the electromagnetic equation. The problem used in this demonstration is designed to mimic that which would be found in a typical borehole measurement calculation. This is in order that it provides a true guidance on the method's capabilities for realistic applications. The problem domain is presented in Figure 3, this has a 2D axi-symmetric (i.e. (r,z)) geometry and is of size 2 metres (m) in radius and 4 metres in height. The domain is layered horizontally in the sense that the material properties (i.e. the electrical conductivities) only vary as a function of height. In this example there are seven layers in total, these are labelled levels 0–6 and are ordered with increasing levels of depth. Layers 0 and 6 are the thickest, and both cover a vertical depth of 1.825 metres. The middle section of the domain is occupied by layers 1–5, and each of these has a depth of 0.07 metres.

The electromagnetic equation was solved in order to find the vector potential $A_\Phi(r, z)$. As explained earlier these were generated through the COMSOL model, and this applied a mesh consisting of 10,929 triangular elements and 111,081 nodes. These solutions provided the full model solutions used to form the snapshots in order to generate the POD model. In total 27 solutions were generated, and for each a different set of electrical material properties was used in the problem's layers. The material properties for each calculation are summarised in Table 1. Their values were varied within layers 1–5 with magnitude between 0.001 and 1 S/m, which is the typical range of material properties found in these applications. In layers 0 and 6 the properties were fixed with value 0.016 S/m. For all simulations, to initiate the electromagnetic field, an electrical

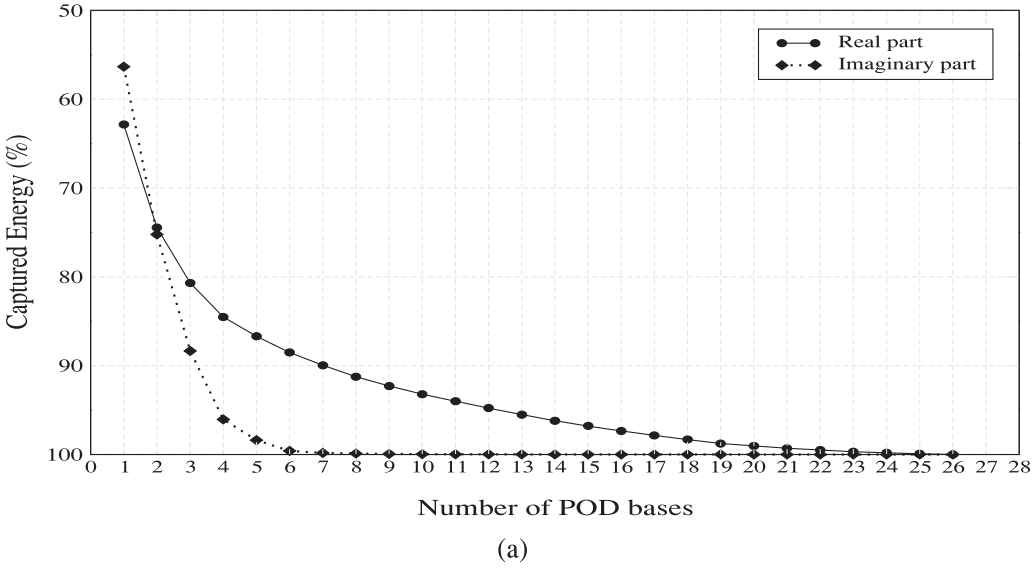

(a)

Figure 4. Energy percentage captured by POD basis for real and imaginary parts. In our case, we choose 20 POD basis functions which can capture 99% energy from the real part and 99.99% energy from the imaginary part.

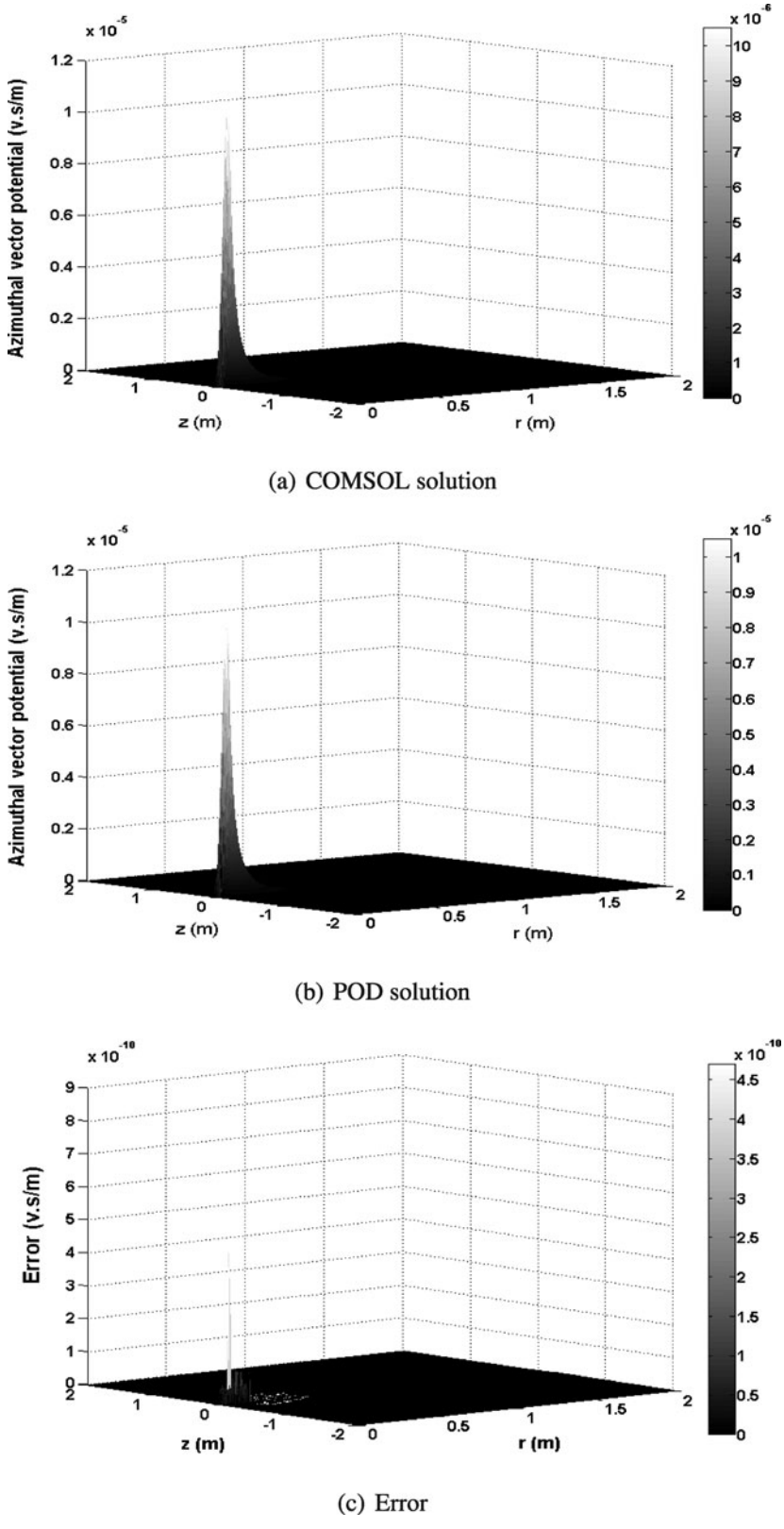

Figure 5. Comparison of the real part of azimuthal vector potential between the full model (a) and the reduced model (b) for a seen case with conductivities of 0.03, 0.03, 0.001, 1 and 0.001 S/m for each layer. (c) The error between the forward and POD solutions.

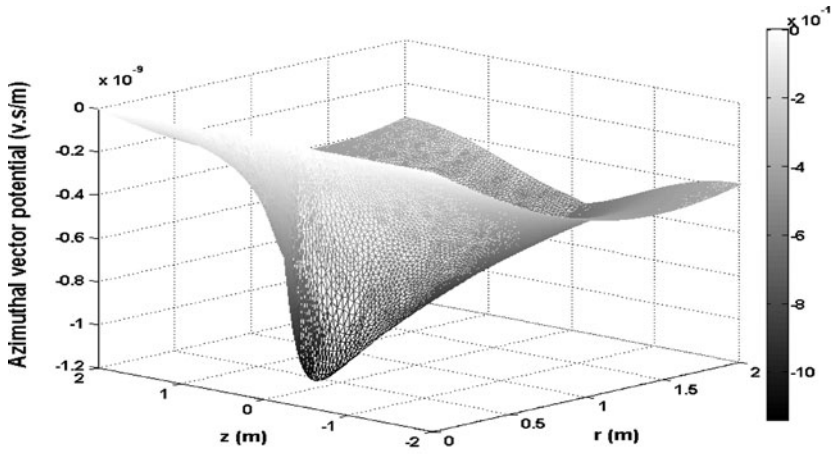

(a) COMSOL solution

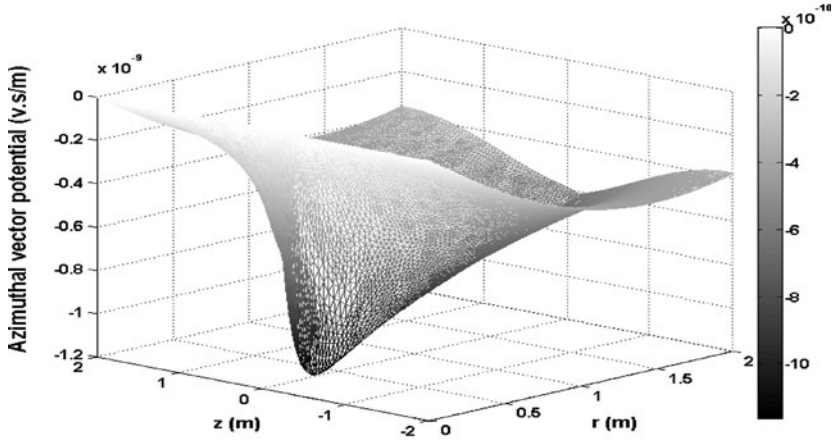

(b) POD solution

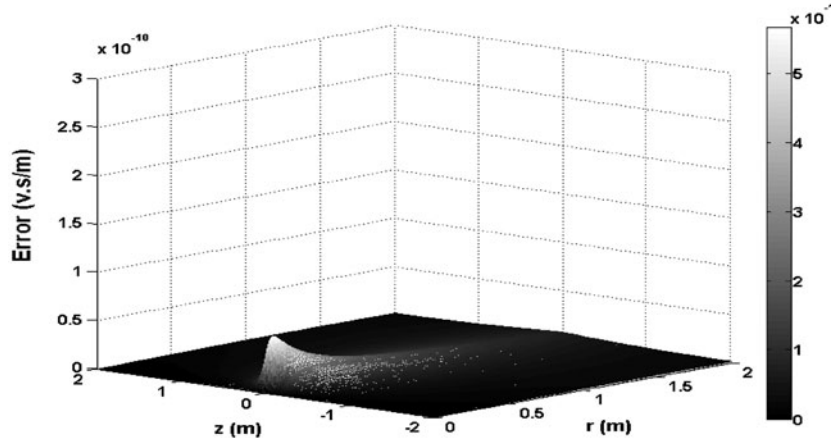

(c) Error

Figure 6. Comparison of the imaginary part of azimuthal vector potential between the full model (a) and the reduced model (b) for a seen case with conductivities of 0.03, 0.03, 0.001, 1 and 0.001 S/m for each layer. (c) The error between the forward and POD solutions.

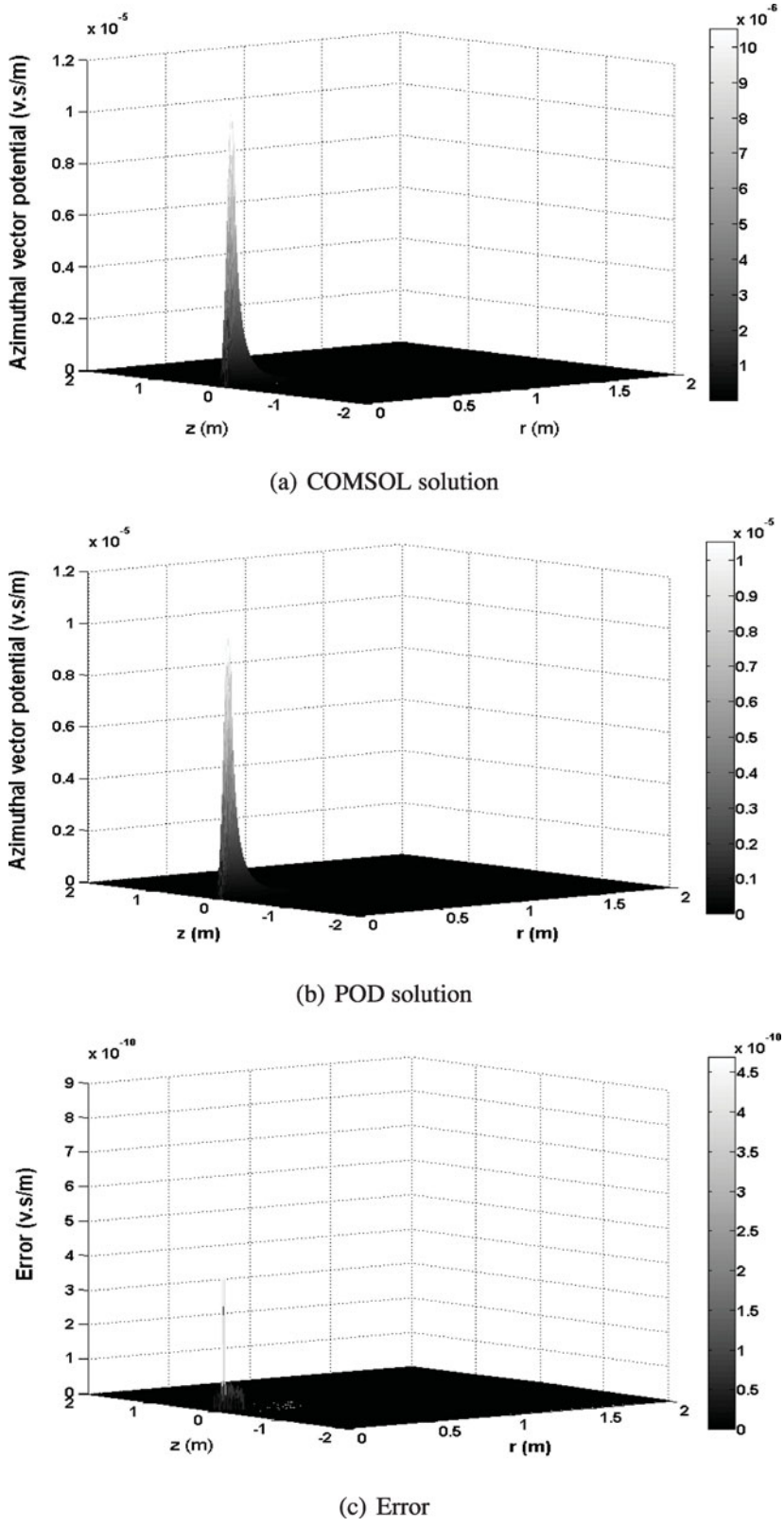

Figure 7. Comparison of the real part of azimuthal vector potential between the full model (a) and the reduced model (b) for an unseen case with conductivities of 0.025, 0.033, 0.08, 0.09 and 0.09 S/m for each layer. (c) The error between the forward and POD solutions.

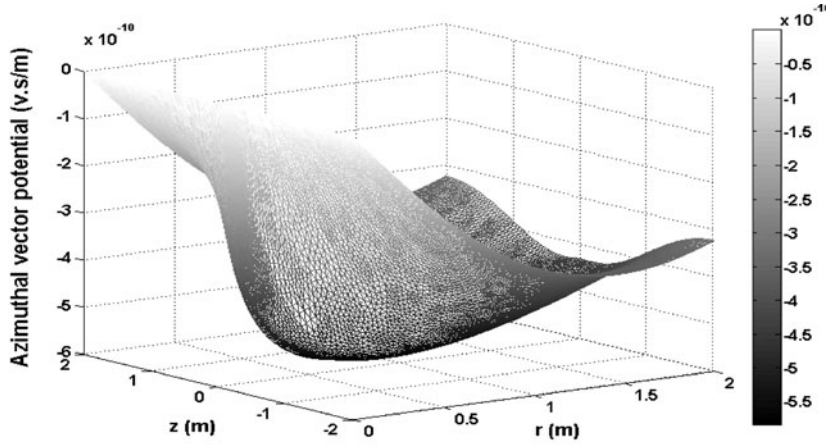

(a) COMSOL solution

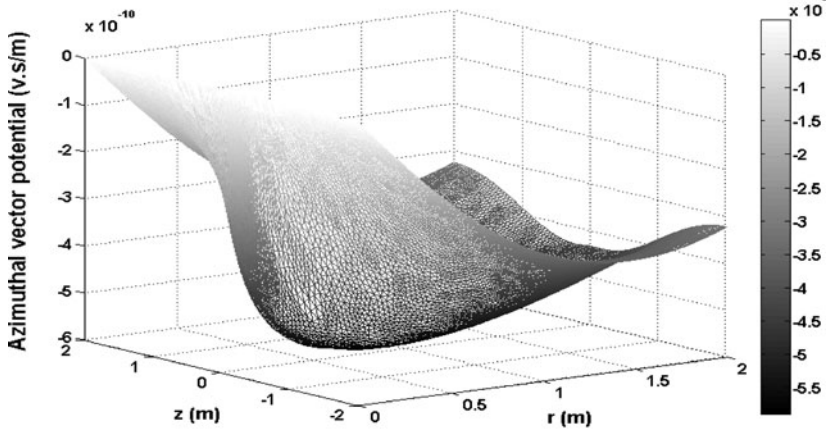

(b) POD solution

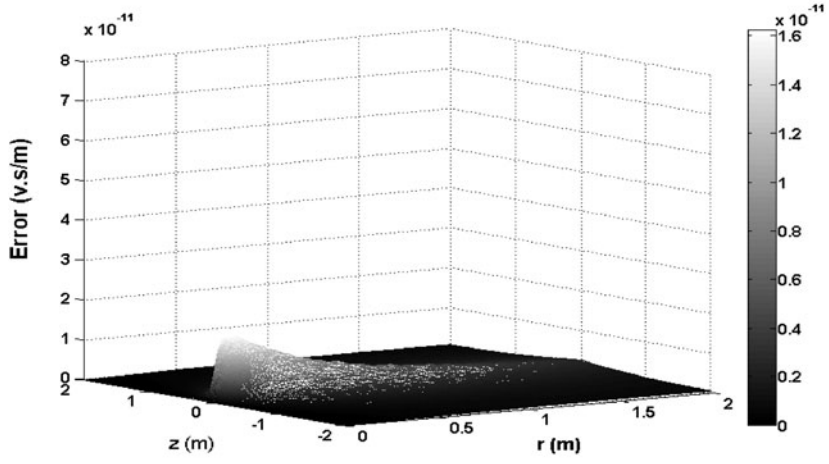

(c) Error

Figure 8. Comparison of the imaginary part of azimuthal vector potential between the full model (a) and the reduced model (b) for an unseen case with conductivities of 0.025, 0.033, 0.08, 0.09 and 0.09 S/m for each layer. (c) The error between the forward and POD solutions.

source was used which is of a type similar to that generated by an induction tool. This source is positioned horizontally in the centre of the domain at $r = 0$, and has a depth so that it is positioned in the middle of layer 4. For all calculations the Dirichlet boundary $A_\phi = 0$ was applied to the domain's central axis at $r = 0$.

The snapshot matrices, POD functions and resulting reduced order models were generated for the real and imaginary solution parts using the methods described in the previous sections. The graph presented in Figure 4 shows the energy values from the resulting POD basis vectors generated for both real and imaginary snapshot sets. It is shown that with just five POD functions 98% of the imaginary solution data and 86.68% of the real solution data are captured. Using 20 POD basis functions the energy captured increases to 99% (real) and 99.99% (imaginary).

The profiles presented in Figures 5–8 compare the results and absolute differences between the COMSOL and POD model solutions. In the POD model calculations, 20 POD basis functions were used to resolve both the real and imaginary parts of its solution (as this generates a 40×40 matrix, a simple direct solver is used). Figures 5

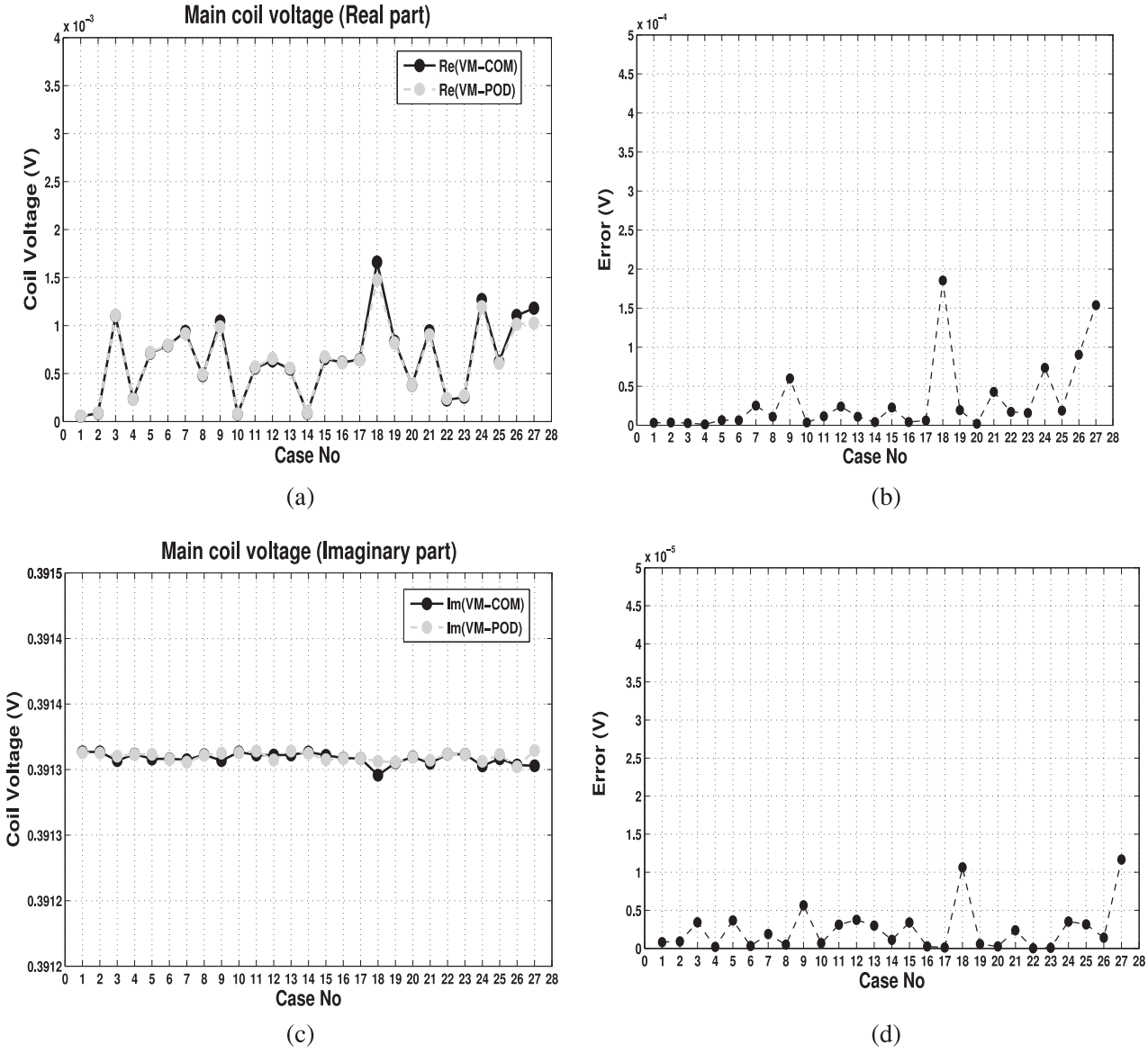

Figure 9. Comparison between the real part (a) and imaginary part (c) of the voltages of main coil calculated from COMSOL and POD solutions for 27 snapshots (Table 1) that are used to obtain the POD basis functions. (b) and (d) show the absolute error between the calculated voltages from POD and COMSOL solutions.

and 6 compare the solutions for a problem with material properties identical to one of those used in creating the snapshot data – case 13 in Table 1. In this case the two sets of solutions are in very close agreement. Figures 7 and 8 present the solutions from both models to a problem with material properties that vary from those used to generate the snapshot sets (the conductivities of layers 1–5 were set to 0.025, 0.033, 0.08, 0.09 and 0.09 S/m, respectively). Again the POD model has performed well as both sets of solutions are in close agreement. This close agreement is supported by the fact that the maximum difference between the COMSOL and POD model solutions is less than 0.4×10^{-11}, for real part, and 0.4×10^{-12} for imaginary part.

To further quantify the accuracy of the POD model, voltages have been estimated from its solution across the main and bucking coils. These are positioned along the central vertical axis of the problem, as shown in Figure 3, and sit within layer 3, for bucking coil, and layer 2, for main coil. The voltage is calculated from the formula

$$V = i\omega \frac{N_R}{h} \int_{\text{line}} 2\pi\rho A_\phi dz, \tag{29}$$

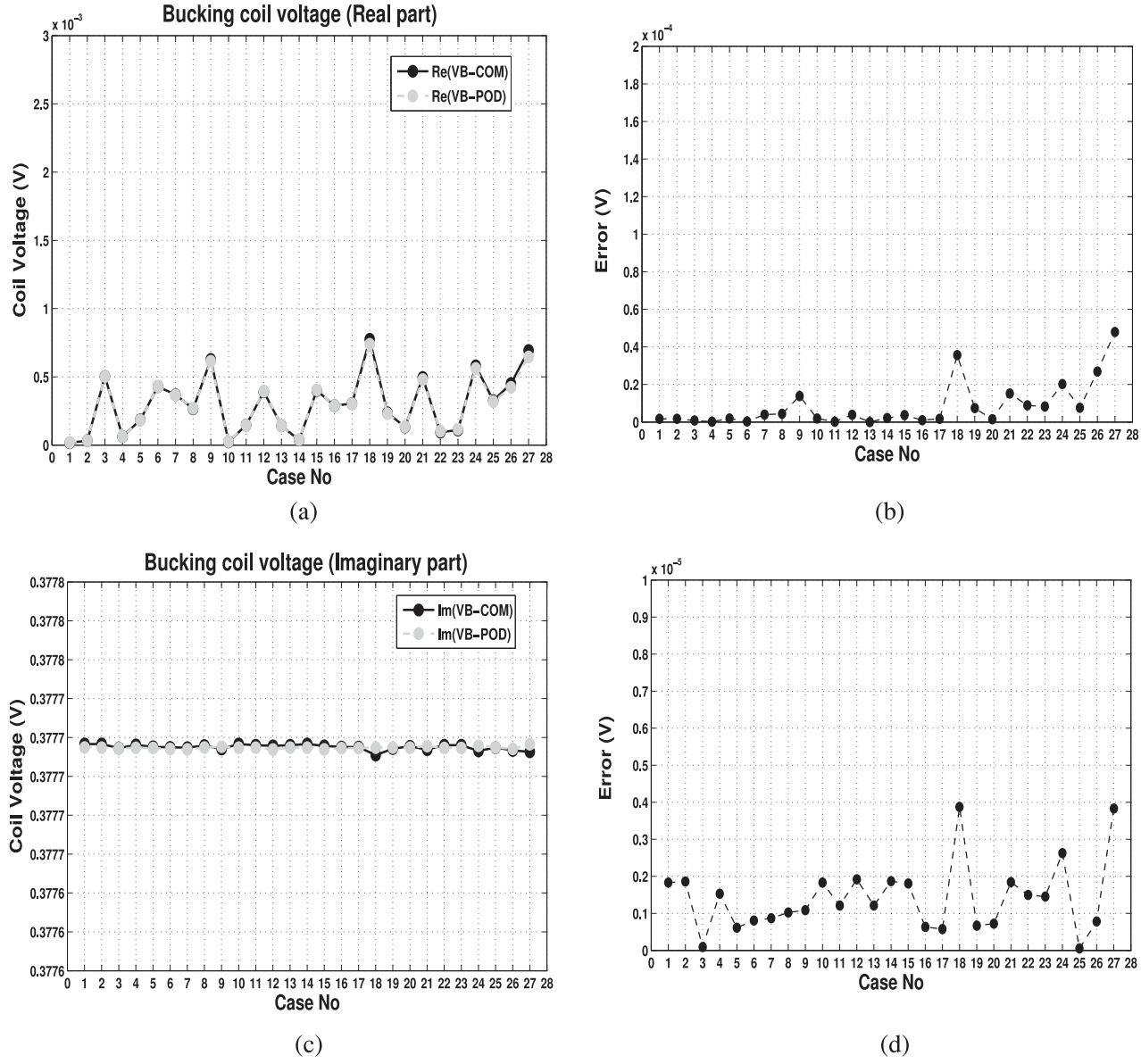

Figure 10. Comparison between the real (a) and imaginary (c) parts of voltages of bucking coil calculated from COMSOL and POD solutions for 27 snapshots (Table 1) that are used to obtain the POD basis functions. (b) and (d) show the absolute error between the estimated voltages from POD and COMSOL solutions.

where h denotes the coil's length and z is the vertical coordinate. The integral is taken over the line representing the cylindrical surface of the coil.

Figures 9 and 10 present graphs that show the voltage solutions, both the real and imaginary parts, and their differences as calculated by the COMSOL and POD models. These results were generated by solving the 27 problem domains used in generating the snapshot data sets. For the majority of cases, particularly with low conducting materials, the absolute difference in the real solutions between the two models is below 0.5×10^{-4} S/m in the main coil, and 0.5×10^{-6} S/m within the bucking coil – this variation is within 6%. For higher conductivities, in particular cases 18 and 27, there are larger errors. The imaginary parts of the voltage are resolved accurately by the POD model. Typically the difference remains below 1.5×10^{-5} S/m (within the main coil) and 3.8×10^{-6} S/m (within the bucking coil) which is a less than 1% variation between the two model predictions.

The voltages were also calculated for problems with material properties different from those used in generating the snapshot data. In total 22 problem domains were

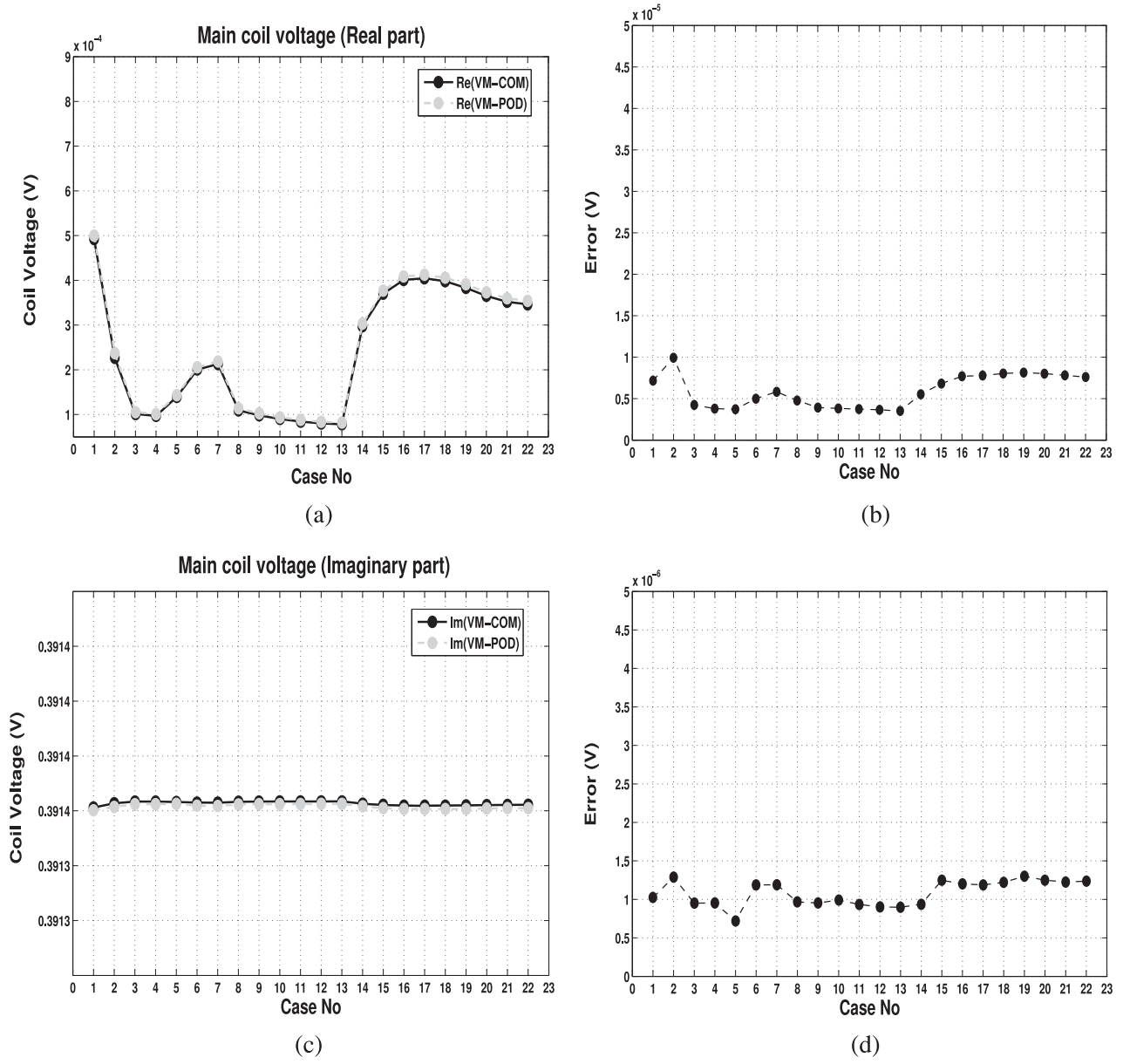

Figure 11. Comparison between the real (a) and imaginary (c) parts of the voltages of main coil calculated from COMSOL and POD solutions for unseen cases (Table 2). (b) and (d) show the absolute error between the calculated voltages from POD and COMSOL solutions.

resolved, the corresponding material properties are listed in Table 2. The voltages calculated by the POD and COMSOL models, and their differences, are presented in Figures 11 and 12. Again there is good agreement between the two model predictions. For the real part of the solution the difference remains below 5×10^{-6} S/m for both coils, for the imaginary part the difference does not exceed 2×10^{-6}. The voltages in the main and bucking coils have been predicted to be within 6% (real) and 1% (imaginary) of each other, respectively.

The computational times for executing the various procedures in the formulation of the POD model have been recorded. The time to compute the reduced order 'reference matrices' used in Equation (26) was found to be in the region of around 100 seconds. This was the most expensive component; however, as this is a pre-processing step it is only required to be computed once. The generation and solving of the reduced order system requires less than a second. This is exceptionally fast in comparison to solving the full model, this is required in the region of 60–70 seconds per solution.

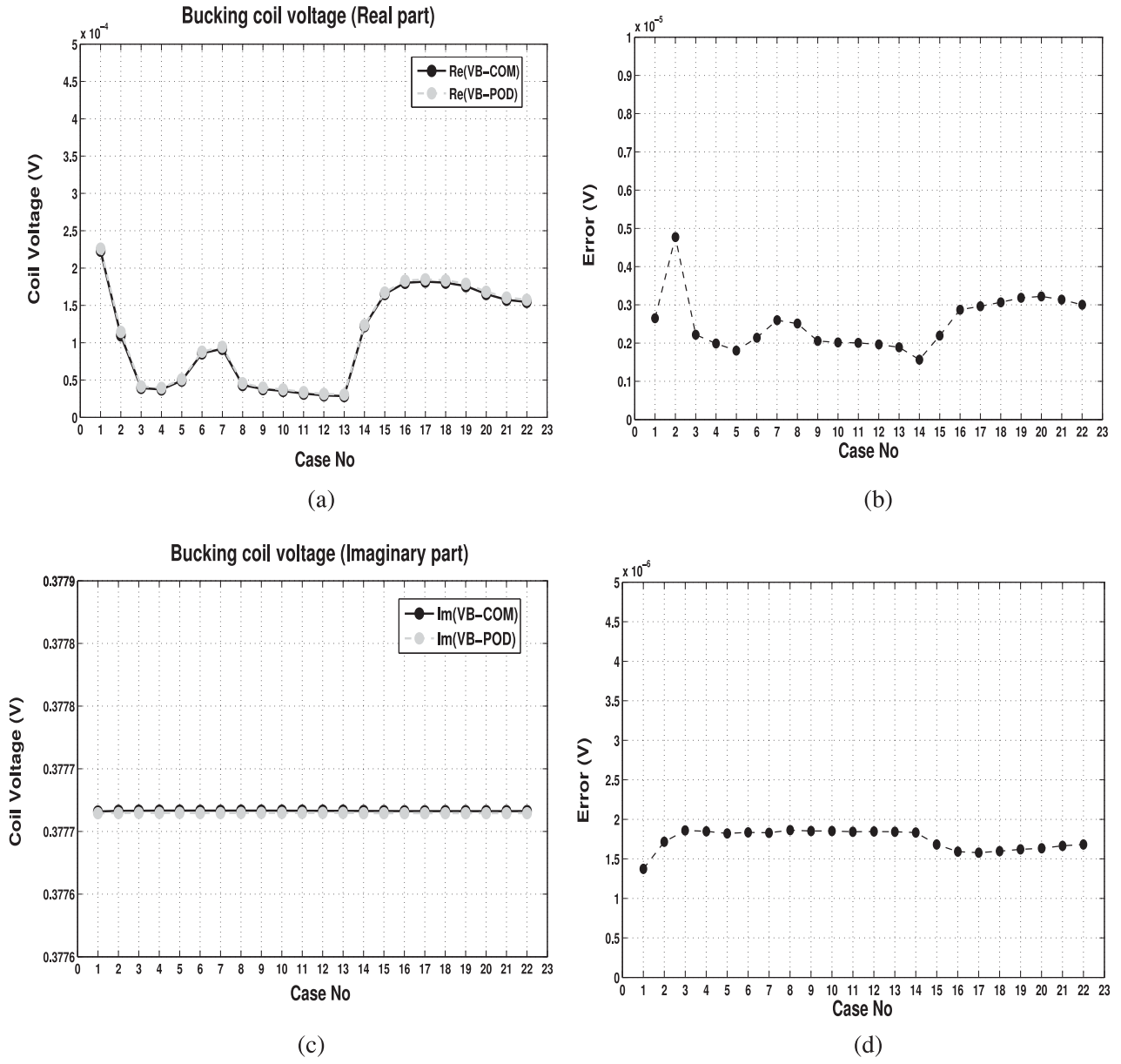

Figure 12. Comparison between the real (a) and imaginary (c) parts of the voltages of bucking coil calculated from COMSOL and POD solutions for unseen cases (Table 2). (b) and (d) show the absolute error between the calculated voltages from POD and COMSOL solutions.

Table 2. The conductivity of the each layer for unseen cases.

No of cases	Layer 1	Layer 2	Layer 3	Layer 4	Layer 5
1	0.25	0.25	0.25	0.25	0.25
2	0.25	0.22	0.05	0.025	0.025
3	0.05	0.025	0.025	0.025	0.025
4	0.025	0.025	0.025	0.025	0.025
5	0.025	0.025	0.03	0.08	0.09
6	0.03	0.08	0.09	0.09	0.09
7	0.09	0.09	0.09	0.09	0.09
8	0.08	0.03	0.025	0.025	0.025
9	0.03	0.025	0.025	0.025	0.025
10	0.025	0.025	0.025	0.015	0.014
11	0.025	0.023	0.015	0.014	0.014
12	0.023	0.015	0.014	0.014	0.014
13	0.015	0.014	0.014	0.014	0.014
14	0.014	0.03	0.17	0.2	0.2
15	0.03	0.17	0.2	0.2	0.2
16	0.017	0.2	0.2	0.2	0.2
17	0.2	0.2	0.2	0.2	0.2
18	0.2	0.2	0.2	0.19	0.17
19	0.2	0.2	0.19	0.17	0.16
20	0.2	0.19	0.17	0.16	0.16
21	0.19	0.17	0.16	0.16	0.16
22	0.17	0.16	0.16	0.16	0.16

5. Conclusions

This paper has presented a new method for an efficient 'forward model' solution of the electromagnetic equation that may be used in borehole measurement calculations. This is based on a reduced order model that uses the method of POD in conjunction with the method of snapshots. This approach uses the solutions of the electromagnetic equation generated from a high resolution (or full) model, in this article COMSOL was employed. These solutions form snapshots of the vector potential, which in turn were used to form the POD basis functions. These functions are optimal in the sense that they can efficiently capture the energy of the snapshot data. The result is that when used to form a new discretised model, only a small number of functions were required. This meant that linear system generated by POD was significantly smaller in size in comparison to the original full model, thus it was more efficient to solve. The novelty of this article is in the use of POD for the application of solving the electromagnetic equation, and with it being used to resolve the real and imaginary parts of its solution. It has also been shown how the reduced order models can be generated efficiently.

A demonstration in the capabilities of the POD model has been presented by solving a problem similar to that found in borehole measurement calculations. Here a layered formation of the problem was represented in axi-symmetric geometry for which the layer's conductivities were varied across the range of values seen in typical problems. Using just 27 snapshots and 20 POD basis functions the reduced order model could capture more that 99% of the real and 99.99% imaginary parts of the energy. This was reflected in the results as there was close agreement in the solutions calculated by the POD and COMSOL models. This was demonstrated by solving problems that were used in generating the snapshot set, and also problems that were not. In both cases the POD model accurately resolved these domains and provided significant improvement in efficiency though a reduction in the computational time. Problem sizes between the full models and POD were reduced by four orders of magnitude.

Acknowledgements

We wish to thank British Petroleum (BP) for their support.

Funding

Prof. I.M. Navon would like to acknowledge support from National Science Foundation (NSF) [grant number ATM-0931198]. We also wish to acknowledge support from Natural Environment Research Council (NERC) [grant number NE/J015938/1]; the Engineering Physical Science Research Council (EPSRC) [grant number EP/I00405X/1], [grant number EP/J002011/1]. We thank Dr R. Stefanescu for sharing DEIM expertise.

Note

1. http://www.comsol.com

References

Anderson, B. I. 2001. "Modeling and Inversion Methods for the Interpretation of Resistivity Logging Tool Response." PhD thesis, Technische Universiteit Delft.

Anderson, B., and S. Gianzero. 1983. "Induction Sonde Response in Stratified Media." *The Log Analyst* 24(1): 25–31.

Ardjmandpour, N. 2010. "Modelling and Inversion of Array Induction Tool." PhD thesis, Imperial College London.

Aubry, N., P. Holmes, and J. L. Lumley. 1988. "The Dynamics of Coherent Structures in the Wall Region of a Turbulent Boundary Layer." *Journal of Fluid Dynamics* 192: 115–173.

Banks, H. T., M. L. Joyner, B. Wincheski, and W. P. Winfree. 2000. "Nondestructive Evaluation Using a Reduced-Order Computational Methodology." *Inverse Problems* 16(4): 929–945.

Barber, T. D., T. Broussard, G. N. Minerbo, D. Murgatroyd, and Z. Sijercic. 1999. "Interpretation of Multiarray Induction Logs in Invaded Formations at High Relative Dip Angles." *The Log Analyst*, 40(3): 220–217.

Barber, T. D., and R. A. Rosthal. 1991. "Using a Multiarray Induction Tool to Achieve High-Resolution Logs with Minimum Environmental Effects." SPE Annual Technical Conference and Exhibition, Dallas, TX.

Cao, Y., J. Zhu, I. M. Navon, and Z. Luo. 2007. "A Reduced-Order Approach to Four-Dimensional Variational Data Assimilation Using Proper Orthogonal Decomposition." *International Journal for Numerical Methods in Fluids* 53(10): 1571–1583.

Carlberg, K., C. Farhat, J. Cortial, and D. Amsallem. 2013. "The {GNAT} Method for Nonlinear Model Reduction: Effective Implementation and Application to Computational Fluid Dynamics and Turbulent Flows." *Journal of Computational Physics* 242(0): 623–647.

Chaturantabut, S., and D. Sorensen. 2010. "Nonlinear Model Reduction via Discrete Empirical Interpolation." *SIAM Journal on Scientific Computing* 32: 2737–2764.

Chen, X., I. M. Navon, and F. Fang. 2011. "A Dual-Weighted Trust-Region Adaptive POD 4D-VAR Applied to a Finite-Element Shallow Water Equations Model." *International Journal for Numerical Methods in Fluids* 65(5): 520–541.

Crommelin, D. T., and A. J. Majda. 2004. "Strategies for Model Reduction: Comparing Different Optimal Bases." *Journal of the Atmospheric Sciences* 61(17): 2206–2217.

Daescu, D. N., and I. M. Navon. 2008. "A Dual-Weighted Approach to Order Reduction in 4DVAR Data Assimilation." *Monthly Weather Review* 136(3): 1026–1041.

Doll, H. G. 1949. "Introduction to Induction Logging and Application to Logging of Wells Drilled with Oil Base Mud." *Journal of Petroleum Technology* 1: 148–162.

Dyos, C. J. 1987. "Inversion of Induction Log Data by the Method of Maximum Entropy," Transactions of the SPWLA 28th Annual Logging Symposium, London, England, June 29–July 2, 1987.

Ellis, D. V., and J. M. Singer. 2007. *Well Logging for Earth Scientists*. Dordrecht: Springer.

Fang, F., C. C. Pain, I. M. Navon, G. J. Gorman, M. D. Piggott, and P. A. Allison. 2011. "The Independent Set Perturbation Adjoint Method: A New Method of Differentiating Mesh-Based Fluids Models." *International Journal for Numerical Methods in Fluids* 66(8): 976–999.

Fang, F., C. C. Pain, I. M. Navon, M. D. Piggott, G. J. Gorman, P. A. Allison, and A. J. H. Goddard. 2009. "Reduced Order Modelling of an Adaptive Mesh Ocean Model." *International Journal for Numerical Methods in Fluids* 59: 827–851.

Freedman, R., and G. N. Minerbo. 1991. "Maximum Entropy Inversion of Induction-Log Data." *SPE Formation Evaluation* 6: 259–268.

Fukunaga, K. 1990. *Introduction to Statistical Pattern Recognition*. *Computer Science and Scientific Computing Series*. 2nd ed. Boston, MA: Academic Press.

Grove, G. P., and G. N. Minerbo. 1991. "An Adaptive Borehole Correction Scheme for Array Induction Tools." Society of Professional Well Log Analysts Logging Symposium, Midland, Texas, Paper P, 1–25.

Gunzburger, M. D. 2003. *Perspectives in Flow Control and Optimization*. SIAM. Philadelphia, USA.

Hardman, R. H., and L. C. Shen. 1987. "Charts for Correcting the Effect of Formation Dip and Hole Deviation on Induction Logs." *The Log Analyst* 28 (4): 349–356.

Holmes, P., J. L. Lumley, and G. Berkooz. 1998. *Turbulence, Coherent Structures, Dynamical Systems and Symmetry*. Vol. 192. Cambridge: Cambridge University Press.

Hopcroftand, P. O., K. Gallagher, C. C. Pain, and F. Fang. 2009. "Three-Dimensional Simulation and Inversion of Borehole Temperatures for Reconstructing Past Climate in Complex Settings." *Journal of Geophysical Research* 114: 1–16. F02019, doi:10.1029/2008JF001165.

Hoteit, I., and A. Köhl. 2006. "Efficiency of Reduced-Order, Time-Dependent Adjoint Data Assimilation Approaches." *Journal of Oceanography* 62(4): 539–550.

Howard, A. Q. 1992. "A New Invasion Model for Resistivity Log Interpretation." *Log Analyst* 33(2): 96–110.

Jolliffe, I. T. 2002. *Principal Component Analysis*. 2nd ed. Dordrecht: Springer.

Karhunen, K. 1946. "Zur Spektraltheorie stochastischer Prozesse." *Annales Academiae Scientiarum Fennicae* Ann. Acad. Sci. Fennicae. Ser. A. I. Math.-Phys. 37: 1–79.

Kirby, M., and L. Sirovich. 1990. "Application of the Karhunen-Loève Procedure for the Characterization of Human Faces." *IEEE Transactions on Pattern Analysis and Machine Intelligence* 12: 103–108.

Kosambi, D. D. 1943. "Statistics in Function Space." *Journal of the Indian Mathematical Society* 7: 76–88.

Kunisch, K., and S. Volkwein. 2010. "Optimal Snapshot Location for Computing Pod Basis Functions." *ESAIM: Mathematical Modelling and Numerical Analysis* 44: 509–529.

Liao, C.-M., B. Balachandran, M. Karkoub, and Y. L. Abdel-Magid. 2011. "Drill-String Dynamics: Reduced-Order Models and Experimental Studies." *ASME Journal of Vibration and Acoustics* 133(4): 041008-1–041008-8.

Lin, Y.-Y., S. Gianzera, and R. Strickland. 1984. "Inversion of Induction Logging Data Using the Least Squares Technique." SPWLA 25th Annual Logging Symposium Transactions. Society of Professional Well Log Analysts, New Orleans, Louisiana, June 10–13.

Loève, M. 1945. "Sur les fonctions aleatoires stationaires du second ordre." *Revue Scientifique* 83: 297–303.

Lumley, J. L. 1967. The structure of inhomogeneous turbulent flows. In Atmospheric Turbulence and Radio Propagation. Nauka: Moscow, 166–178.

Luo, Z., J. Chen, J. Zhu, R. Wang, and I. M. Navon. 2007. "An Optimizing Reduced Order FDS for the Tropical Pacific Ocean Reduced Gravity Model." *International Journal for Numerical Methods in Fluids* 55(2): 143–161.

Luo, Z., J. Zhu, R. Wang, and I. M. Navon. 2007. "Proper Orthogonal Decomposition Approach and Error Estimation of Mixed Finite Element Methods for the Tropical Pacific Ocean Reduced Gravity Model." *Computer Methods in Applied Mechanics and Engineering* 196(41–44): 4184–4195.

Majda, A. J., I. Timofeyev, and E. Vanden-Eijnden. 2003. "Systematic Strategies for Stochastic Mode Reduction in Climate." *Journal of the Atmospheric Sciences* 60(14): 1705–1722.

Moran, J. H. 1982. "Induction Logging-Geometrical Factors with Skin Effect." *The Log Analyst* 23(6): 4–10.

Pearson, K. 1901. "On Lines and Planes of Closest Fit to Systems of Points in Space." *Philosophical Magazine* 2(6): 559–572.

Razvan, Stefanescu, & I.M. Navon: 2005. "POD/DEIM Nonlinear model" order reduction of an ADI implicit shallow water equations model. *Journal of Computational Physics* 237: 95–114.

Robert, C., S. Durbiano, E. Blayo, J. Verron, J. Blum, and F.-X. L. Dimet. 2005. "A Reduced-Order Strategy for 4d-Var Data Assimilation." *Journal of Marine Systems* 57(1–2): 70–82.

Rust, D., and B. Anderson. 1975. "An intimate look at induction logging". *The Technical Review* 23(2): 30–54.

Sirovich, L. 1987. "Turbulence and the Dynamics of Coherent Structures, Part III: Dynamics and Scaling." *Quarterly of Applied Mathematics* XLV: 583–590.

Thadani, S. G., G. A. Merchant, and J. L. Verbout. 1983. "Deconvolution with Variable Frequency Induction Logging Systems." SPWLA Twenty Fourth Annual Logging Symposium, Calgary, Alberta, June 27–30.

Vauhkonen, M., J. P. Kaipio, E. Somersalo, and P. A. Karjalainen. (1997). "Electrical Impedance Tomography with Basis Constraints." *Inverse Problems* 13 (2): 523–530.

Willcox, K., and J. Peraire. 2002. "Balanced Model Reduction via the Proper Orthogonal Decomposition." *AIAA Journal* 40: 2323–2330.

Xiao, D., F. Fang, A. Buchan, C. Pain, I. Navon, J. Du, and G. Hu. 2014. "Non-linear Model Reduction for the Navier—Stokes Equations Using Residual {DEIM} Method." *Journal of Computational Physics* 263(0): 1–18.

Xiao, J., I. Geldmacher, and M. Rabinovich. 2000. "Deviated-Well Software Focusing of Multiarray Induction Measurements." SPWLA 41st Annual Logging Symposium, Dallas, Texas, June 4–7.

Xu, H. 2005. "A Catalogue of Three-Level Regular Fractional Factorial Designs." *Metrika* 62(2): 259–281.